Inorg. Chem. **2008**, *47*, 5831−5840

Inorganic Chemistry
Article

$Sn_{12}O_8(OH)_4(OEt)_{28}(HOEt)_4$: an Additional Member in the Family of Dodecameric Oxo Clusters

F. Ribot,*,† E. Martinez-Ferrero,† K. Boubekeur,‡ P. M. S. Hendrickx,§ J. C. Martins,§ L. Van Lokeren,⊥ R. Willem,⊥ and M. Biesemans⊥

Chimie de la Matière Condensée de Paris, UPMC Universite Paris 06, UMR 7574, T54-E5, 4 place Jussieu, F-75252 Paris, France, Chimie Inorganique et Matériaux Moléculaires, UPMC Universite Paris 06, UMR 7071, F74-E4, 4 place Jussieu, F-75252 Paris, France, NMR and Structure Analysis Unit, Vakgroep Organische Chemie, Universiteit Gent, Krijgslaan 281 S4, B-9000 Gent, Belgium, and High Resolution NMR centre, Vrije Universiteit Brussel, Pleinlaan 2, B-1050 Brussel, Belgium

Received January 23, 2008

A tin(IV) oxoalkoxo cluster with unprecedented architecture has been prepared and characterized by single-crystal X-ray diffraction. The cluster obeys the formula $Sn_{12}O_8(OH)_4(OEt)_{28}(HOEt)_4$ (**1**) and is based on an elongated centrosymmetric assembly of 12 six-coordinate tin centers, 28 peripheral ethoxy groups (terminal and bridging), 8 oxo bridges (μ_2 and μ_3), 4 hydroxy bridges (μ_2), and 4 ethanol molecules that are all bound to tin atoms and interact strongly, through hydrogen bonds, with an ethoxy group located on a vicinal tin atom. This compound has also been fully characterized in solution by multinuclear 1D and 2D NMR, with all of its ^{119}Sn, ^{1}H, and ^{13}C NMR resonances assigned with respect to the structure. Altogether, the data allowed unambiguous location of the hydroxy groups. Information on the exchange of the ethoxy groups is also presented.

1. Introduction

Dodecameric oxo clusters form a large family in which the Keggin's type polyoxometallates $[XM_{12}O_{40}]^{n-}$ (M = W, Mo; for X = Si^{IV}, $n = 4$; for X = P^{V} or As^{V}, $n = 3$; for X = Co^{II}, $n = 6$)[1] and the manganese-based single-molecule magnet $[Mn_{12}O_{12}(O_2CR)_{16}(H_2O)_4]$ are among the best known.[2] The number of metallic centers is not the only feature shared by the members of this family. For example, the metal−oxo framework depicted in Figure 1 is adopted by several members: $Ti_{12}O_{16}(OEt)_{16}$,[3] $\{(VO)_{12}O_{12}F_2(OH)_6\}^{6-}$,[4] $\{(RSn)_{12}O_{14}(OH)_6\}^{2+}$ (R = ^{i}Pr, Bu, CH_2SiMe_3),[5] and $\{(^{i}PrSn)_{11}(VO)O_{14}(OH)_6\}^{+}$.[6]

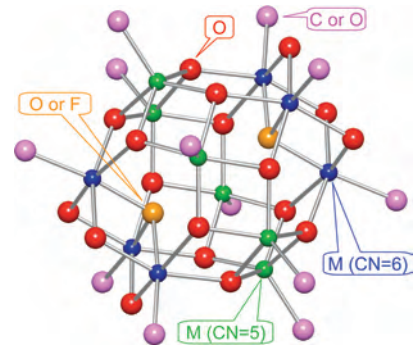

Figure 1. Representation of the metal−oxo framework adopted by $Ti_{12}O_{16}(OEt)_{16}$,[3] $\{(VO)_{12}O_{12}F_2(OH)_6\}^{6-}$,[4] $\{(RSn)_{12}O_{14}(OH)_6\}^{2+}$ (R = ^{i}Pr, Bu, CH_2SiMe_3),[5] and $\{(^{i}PrSn)_{11}(VO)O_{14}(OH)_6\}^{+}$.[6]

* To whom correspondence should be addressed. E-mail: francois.ribot@courriel.upmc.fr.
† UPMC Universite Paris 06, UMR 7574, CMCP.
‡ UPMC Universite Paris 06, UMR 7071, CIM2.
§ Universiteit Gent.
⊥ Vrije Universiteit Brussel.

(1) (a) *Polyoxometalate chemistry: from topology via self-assembly to applications*; Pope, M. T., Müller, A., Eds.; Kluwer Academic Publishers: Dordrecht, The Netherlands, 2001. (b) *Polyoxometalates Chemistry for Nano-composite Designs*; Yamase, T., Pope, M. T., Eds.; Kluwer Academic/Plenum Publishers: New York, 2002. (c) Pope, M. T. In *Comprehensive Coordination Chemistry II*; McCleverty, J. A., Meyer, T. J., Eds.; Elsevier: Oxford, U.K., 2004; pp 635−678. (d) Hill, C. L. In *Comprehensive Coordination Chemistry II*; McCleverty, J. A., Meyer, T. J., Eds.; Elsevier: Oxford, U.K., 2004; pp 679−759.
(2) (a) Lis, T. *Acta Crystallogr.* **1980**, *B36*, 2042–2046. (b) Christou, G. *Polyhedron* **2005**, *24*, 2065–2075.
(3) (a) Day, V. W.; Eberspacher, T. A.; Klemperer, W. G.; Park, C. W. *J. Am. Chem. Soc.* **1993**, *115*, 8469–8470. (b) Steunou, N.; Robert, F.; Boubekeur, K.; Ribot, F.; Sanchez, C. *Inorg. Chim. Acta* **1998**, *279*, 144–151.
(4) Müller, A.; Rohlfing, R.; Krickemeyer, E.; Bögge, H. *Angew. Chem., Int. Ed. Engl.* **1993**, *32*, 909–912.

10.1021/ic800123z CCC: $40.75
Published on Web 06/03/2008

Contrary to titanium, for which a unique dodecameric oxo cluster structure has been described (yet with two isomers),[3] tin(IV) contributes more generously to this family. In addition to the monoorganotin oxo clusters with the structure depicted in Figure 1, there are four additional entries: $\{(BuSn)_9(OV)_3O_{14}(OH)_6Cl_2(DMSO)_2\}$, the oxo framework of which is closely related to the one shown in Figure 1,[7] $[Na\subset(^iPrSn)_{12}O_{14}(OH)_{24}]^{5+}$, which exhibits γ-Keggin's structure and includes a sodium cation at its center,[8] $\{[Sn(CH_2)_3Sn]_6O_{10}(OH)_2(O_2CCH_2Cl)_{14}\}$, which consists of bridged stannanes,[9] and $\{(RSn)_8O_{14}(OH)_8(SnOH)_4\}$ (R = 2,4,6-$^iPr_3C_6H_2$), in which the four purely inorganic tin centers are the result of a dearylation process taking place during synthesis.[10] However, despite this diversity, a dodecameric tin oxo cluster without any Sn−C bond is, to the best of our knowledge, neither reported nor mentioned so far in the literature. Yet, according to the structural similarities between $Ti_{12}O_{16}(OEt)_{16}$ and $\{(RSn)_{12}O_{14}(OH)_6\}^{2+}$, a tin oxo cluster with the formula $Sn_{12}O_{16}(OR)_{16}$ can be expected to occur as well.

Even if nuclearities different from 12 are considered, tin(IV) oxo clusters without any Sn−C bond remain a poorly documented topic. So far, only three such species were reported: $Sn_3O(O^iBu)_{10}(HO^iBu)_2$,[11] $Sn_4O_2(OEt)_{10}(acac)_2$,[12] and $[SnO(O^tBu)(OAc)]_6$.[13] This trio constitutes quite a small group, especially when compared to the large family formed by titanium oxo clusters.[14]

These different considerations prompted us to start a systematic exploration of the possibilities to prepare new tin oxoalkoxo clusters through the controlled hydrolysis of tin(IV) alkoxides. This quest had two other thrusts. First, the NMR-friendly nature of tin makes its oxoalkoxo clusters valuable model compounds to study exchange reactions that can take place between free nucleophiles and the alkoxy groups present at the surface of such species.[15] Second, metal−oxo clusters are well-defined entities that can be used as nano building blocks in the development of advanced hybrid organic−inorganic materials.[5f,16,17]

This work reports on a new tin oxoalkoxo cluster, $Sn_{12}O_8(OH)_4(OEt)_{28}(HOEt)_4$ (**1**). Its unprecedented architecture is characterized by single-crystal X-ray diffraction. It is also fully characterized in solution by 1D and 2D multinuclear NMR, enabling us to unambiguously locate the hydroxy groups on the metal−oxo framework.

2. Experimental Section

2.1. Materials. All reactions were carried under an inert atmosphere using Schlenk and vacuum-line techniques. $Sn(O^tBu)_4$ was prepared according to literature methods and purified by vacuum distillation.[18] Crystalline $[Sn(O^iPr)_4\cdot HO^iPr]_2$ was obtained by treating $Sn(O^tBu)_4$ with an excess of isopropyl alcohol and recovered by filtration, before drying under reduced pressure.[18] ^{119}Sn NMR (CP-MAS): −654 ppm.

2.2. Synthesis of $Sn_{12}O_8(OH)_4(OEt)_{28}(HOEt)_4$. A mixture of water (0.022 g, 1.2 mmol) and ethanol (4.0 g, 87 mmol) was added to $[Sn(O^iPr)_4\cdot HO^iPr]_2$ (1.0 g, 1.2 mmol, $H_2O/Sn = 0.5$). The resulting clear solution was stirred for a few minutes and then aged at 65 °C in a tightly closed vial. After 1 week, the solution was cooled to room temperature. A very small quantity of transparent needle-shaped crystals grew after 1 week more (yield ∼ 0.1%).[19] The experiment was reproduced several times. However, because of the very low yield and the sensitivity of **1** to moisture, elemental analyses could not be performed. **1** was characterized by single-crystal X-ray diffraction and multinuclear NMR. ^{1}H NMR (C_6D_6, 303 K) and ^{13}C NMR (C_6D_6, 303 K): see Table 3. ^{119}Sn NMR (C_6D_6, 303 K): −563.5, −594.9, −607.8, −609.0, −625.5, and −648.7 ppm.

2.3. Crystal Structure Determination. A single crystal of moisture-sensitive compound **1** was rapidly selected, mounted onto a glass fiber, and transferred in a cold nitrogen gas stream. Diffraction data were collected on a Nonius Kappa CCD diffractometer at 250 K. Unit cell parameter determination, data collection strategy, and integration were carried out with the Nonius EVAL-

(5) (a) Puff, H.; Reuter, H. *J. Organomet. Chem.* **1989**, *373*, 173–184. (b) Dakternieks, D.; Zhu, H.; Tiekink, E. R. T.; Colton, R. *J. Organomet. Chem.* **1994**, *476*, 33–40. (c) Banse, F.; Ribot, F.; Toledano, P.; Maquet, J.; Sanchez, C. *Inorg. Chem.* **1995**, *34*, 6371–6379. (d) Eychenne-Baron, C.; Ribot, F.; Steunou, N.; Sanchez, C.; Fayon, F.; Biesemans, M.; Martins, J. C.; Willem, R. *Organometallics* **2000**, *19*, 1940–1949. (e) Beckmann, J.; Jurschat, K.; Kaltenbrunner, U.; Rabe, S.; Schurmann, M.; Dakternieks, D.; Duthie, A.; Muller, D. *Organometallics* **2000**, *19*, 4887–4898. (f) Ribot, F.; Veautier, D.; Guillaudeu, S.; Lalot, T. *J. Mater. Chem.* **2005**, *15*, 3973–3978.

(6) Kastner, G.; Reuter, H. *J. Organomet. Chem.* **2000**, *598*, 381–386.

(7) Izaaryene, M.; Kastner, G.; Reuter, H. *Z. Kristallogr.* **2005**, *220*, 622–625.

(8) Reuter, H. *Angew. Chem., Int. Engl. Ed.* **1991**, *30*, 1482–1484.

(9) Zobel, B.; Costin, J.; Vincent, B. R.; Tiekink, E. R. T.; Dakternieks, D. *Dalton Trans.* **2000**, 4021–4022.

(10) Prabusankar, G.; Jousseaume, B.; Toupance, T.; Allouchi, H. *Angew. Chem., Int. Ed.* **2006**, *45*, 1255–1258.

(11) Reuter, H.; Kremser, M. *Z. Anorg. Allg. Chem.* **1992**, *615*, 137–142.

(12) Verdenelli, M.; Parola, S.; Hubert-Pfalzgraf, L. G.; Lecocq, S. *Polyhedron* **2000**, *19*, 20692075.

(13) Caruso, J.; Hampden-Smith, M. J.; Rheingold, A. L.; Yap, G. *Chem. Commun.* **1995**, 157–158.

(14) Rozes, L.; Steunou, N.; Fornasieri, G.; Sanchez, C. *Monatsh. Chem.* **2006**, *137*, 501–528.

(15) Fornasieri, G.; Rozes, L.; Le Calvé, S.; Alonso, B.; Massiot, D.; Rager, M.-N.; Evain, M.; Boubekeur, K.; Sanchez, C. *J. Am. Chem. Soc.* **2005**, *127*, 4869–4878.

(16) (a) Ribot, F.; Sanchez, C. *Comments Inorg. Chem.* **1999**, *20*, 327–371. (b) Sanchez, C.; Soler-Illia, G. J.; de, A. A.; Ribot, F.; Lalot, T.; Mayer, C. R.; Cabuil, V. *Chem. Mater.* **2001**, *13*, 3061–3083. (c) Schubert, U. *Chem. Mater.* **2001**, *13*, 3487–3494. (d) Kickelbick, G.; Schubert, U. *Monatsh. Chem.* **2001**, *13*, 13–30. (e) Kickelbick, G. *Prog. Polym. Sci.* **2003**, *28*, 83–114. (f) Laine, R. M. *J. Mater. Chem.* **2005**, *15*, 3725–3744.

(17) (a) Bocchini, S.; Fornasieri, G.; Rozes, L.; Trabelsi, S.; Galy, J.; Zafeiropoulos, N. E.; Stamm, M.; Gérard, J.-F.; Sanchez, C. *Chem. Commun.* **2005**, 2600–2602. (b) Trabelsi, S.; Janke, A.; Hassler, R.; Zafeiropoulos, N. E.; Fornasieri, G.; Bocchini, S.; Rozes, L.; Stamm, M.; Gerard, J.-F.; Sanchez, C. *Macromolecules* **2005**, *38*, 6068–6078. (c) Rozes, L.; Fornasieri, G.; Trabelsi, S.; Creton, C.; Zafeiropoulos, N. E.; Stamm, M.; Sanchez, C. *Prog. Solid State Chem.* **2005**, *33*, 127–135. (d) Ribot, F.; Lafuma, A.; Eychenne-Baron, C.; Sanchez, C. *Adv. Mater.* **2002**, *14*, 1496–1499.

(18) (a) Thomas, I. M. U.S. Patent 3,946,056, 1976. (b) Chandler, C. D.; Fallon, G. D.; Koplick, A. J.; West, B. O. *Aust. J. Chem.* **1987**, *40*, 1427–1439.

(19) ^{119}Sn NMR spectra of the solutions from which the crystals grow gave little clue on the species present. These spectra consist of one intense and broad resonance at −615 ppm and two minor ones at −606 and −609 ppm. These resonances correspond to six-coordinate tin atoms, and the major one might be related to a trimer with the formula $Sn_3(\mu_3\text{-}O)(\mu_2\text{-}OEt)_3(OEt)_7(HOEt)_2$, similar to the one described in ref 11. Similarly, the hydrolysis of $[Sn(O^iPr)_4\cdot(HO^iPr)]_2$ in THF ($H_2O/Sn = 0.5$) yields a solution, the ^{119}Sn NMR spectrum of which consists of a unique resonance, at −595 ppm, flanked by a pair of coupling satellites [$^2J(^{119}Sn-^{117}Sn) = 225$ Hz] with intensities corresponding to those of a trimer. This compound could not be isolated but likely corresponds to $Sn_3(\mu_3\text{-}O)(\mu_2\text{-}O^iPr)_3(O^iPr)_7(HO^iPr)_2$.

Table 1. Crystallographic Data for $Sn_{12}O_8(OH)_4(OEt)_{28}(HOEt)_4$

formula	$C_{64}H_{168}O_{44}Sn_{12}$
M	3066.5
temp/K	250(2)
cryst syst	triclinic
space group, Z	$P\bar{1}$, 1
a/Å	11.979(6)
b/Å	13.562(8)
c/Å	18.618(9)
α/deg	93.83(8)
β/deg	102.77(6)
γ/deg	104.39(4)
V/Å^3	2834(3)
D_{calcd}/(g/cm^3)	1.796
μ/mm^{-1}	2.667
λ(Mo Kα)/Å	0.71073
Θ_{max}/deg	30.0
reflns [collected/independent/$I > 2\sigma(I)$]	56695/16410/9119
R_{int} (obsd/all)	0.0597/0.0769
param/restraints	506/42
$R(F)$, $R_w(F^2)$ [$I > 2\sigma(I)$][a]	0.0684, 0.0809
$R(F)$, $R_w(F^2)$ (all data)[a]	0.1279, 0.1342
GOF in F^2	1.05

[a] $R(F) = \sum||F_o| - |F_c||/\sum|F_o|$, $R_w(F^2) = [\sum w(|F_o|^2| - |F_c|^2)^2/\sum w(|F_o|^4)]^{1/2}$.

14 suite of programs.[20] The data were corrected for absorption by a multiscan method.[21] The structure was solved by direct methods with *SHELXS-86*,[22] refined by full-matrix least squares on F^2 and completed with *SHELXL-97*.[23] Graphics were carried out with *DIAMOND*.[24] All non-hydrogen atoms were refined with anisotropic displacement parameters. Hydrogen atoms bound to carbon atoms were simply introduced at calculated positions (riding model). The final residual values are given in Table 1 along with details on the crystal, the data collection, and the structure determination.

2.4. NMR Spectroscopy. All spectra were recorded from a sealed sample containing ca. 10 mg of cluster in 0.5 mL of C_6D_6, at 303 K on a Bruker Avance II 700 spectrometer operating at 700.13, 176.05, and 260.92 MHz for ^{1}H, ^{13}C, and ^{119}Sn, respectively. Chemical shifts were referenced to the residual solvent peak and converted to the standard Me_4Si scale by adding 7.15 and 128.0 ppm for ^{1}H and ^{13}C NMR, respectively. For ^{119}Sn, external referencing with $\Xi = 37.290\,665$ MHz was used.[25] All 1D and 2D spectra were recorded using pulse sequences from the standard Bruker pulse library as described in ref 26 unless otherwise mentioned.

ROESY (rotating-frame nuclear Overhauser effect spectroscopy) spectra were recorded using the off-resonance scheme in order to avoid misinterpretation of scalar coupling cross-peaks as exchange peaks.[27] Gradient-selected ^{1}H$-^{119}$Sn HMQC (heteronuclear multiple-quantum correlation) spectra[28,29] were recorded with evolution delays for the $^nJ(^1\text{H}-^{119}\text{Sn})$ couplings set to 10, 33, and 125 ms (50, 15, and 4 Hz). ^{1}H$-^{13}$C and ^{1}H$-^{119}$Sn HSQC (heteronuclear single-quantum correlation) spectra were recorded with adiabatic 180° pulses in phase-sensitive and gradient-selected modes with GARP4 decoupling.[26] For the ^{1}H$-^{119}$Sn pair, the gradient ratio for appropriate coherence selection is 80.00:29.83. The pulse program for the J-HMBC (heteronuclear multiple-bond correlation) experiment was obtained from the NMR Pulse Sequence Library of the Carlsberg Laboratory.[30] The J-HMBC spectrum was recorded using adiabatic 180° pulses for ^{119}Sn and optimized delays for long-range couplings of 3 Hz. A scaling factor κ of 23.86 was used to enlarge the active couplings along F1.

For all 2D experiments, typically 512 t_1 increments of 2K data points, 16 scans each, were recorded, except for the HMBC and J-HMBC spectra, where 32−64 scans were used to improve the signal-to-noise ratio. A relaxation delay of 1 s was used throughout. Processing consisted of suitable apodization using a squared sine bell for magnitude-mode data and a squared cosine bell for phase-sensitive data, followed by zero-filling and Fourier transformation to a 2K × 2K data matrix.

The diffusion experiments were performed by pulsed-field-gradient ^{1}H NMR spectroscopy by means of a BPP-LED (bipolar pulse pairs longitudinal eddy current delay) pulse sequence,[31] with shaped gradient pulses of amplitude G and duration δ modulated as the $G[\sin(t\pi/\delta)]$ function. Experiments were carried out at 298 K without sample spinning on a Bruker Avance II 500 MHz equipped with a Bruker BGU z gradient unit providing a maximum gradient strength of 51 G/cm. The amplitude of the field gradient was varied from 2 to 95% of its maximum value, while the gradient recovery delay (τ) and the eddy current delay (t_e) were fixed at 100 μs and 5 ms, respectively. The diffusion delay (Δ) was set to 25, 50, 100, 200, and 400 ms and the corresponding gradient pulse duration (δ) to 10.0, 5.0, 2.8, 1.6, and 1.0 ms, respectively, in order to achieve an intensity attenuation range of at least 95%.

The DOSY (diffusion ordered spectroscopy) NMR data were processed by inverse Laplace transform (ILT),[32] using a maximum entropy algorithm, *MaxEnt*,[33] as implemented in the Gifa Processing package interfaced with TOPSPIN software. The ILT-MaxEnt 2D DOSY spectra obtained display the negative logarithmic scale of the diffusion coefficient on the vertical axis in f1, and the chemical shift (in ppm), for each measurable moiety of the corresponding diffusing species, on the horizontal f2 axis. The resulting 2D spectrum was integrated over a given resonance range along the chemical shift axis, which provides an intensity function depending only on the $-\log D$ variable. A sum of Gaussian functions was fitted to these data, and the maxima thus obtained were used as the representative diffusion coefficients. The fits allowed us to locate the maxima within ca. 1%, and the relative accuracy of the diffusion coefficients can be estimated around 5%.[34] In all DOSY experiments, the diffusion correlation peak of benzene-d_6 allowed us to correct the viscosity of the sample at 298 K to 0.542 cP, instead of 0.646 cP for pure benzene-d_6.[35]

(20) Duisenberg, A. J. M.; Kroon-Batenburg, L. M. J.; Schreurs, A. M. M. *J. Appl. Crystallogr.* **2003**, *36*, 220–229.
(21) Blessing, R. H. *Acta Crystallogr.* **1995**, *A51*, 33–38.
(22) Sheldrick, G. M. *SHELXS-86, Computer program for structure solution*; University of Gottingen: Gottingen, Germany, 1986.
(23) Sheldrick, G. M. *SHELXL-97, Computer program for structure refinement*; University of Gottingen: Gottingen, Germany, 1997.
(24) Brandenburg, K.; Berndt, M. *Diamond*; Crystal Impact GbR: Bonn, Germany, 1999.
(25) Mason, J. *Multinuclear NMR*; Plenum Press: New York, 1987; pp 625−629.
(26) Berger, S.; Braun, S. *200 and More NMR Experiments*; Wiley VCH: New York, 2004; and references cited herein.
(27) Desvaux, H.; Berthault, P.; Birlirakis, N.; Goldman, M.; Piotto, M. *J. Magn. Reson. A* **1995**, *113*, 47–52.
(28) Martins, J. C.; Kayser, F.; Verheyden, P.; Gielen, M.; Willem, R.; Biesemans, M. *J. Magn. Reson.* **1997**, *124*, 218–222.
(29) Martins, J. C.; Biesemans, M.; Willem, R. *Prog. Nucl. Magn. Reson. Spectrosc.* **2000**, *36*, 271–322.
(30) http://www.crc.dk/nmr/nmrpulse/experiments/small/jhmbc/index.shtml.
(31) Wu, D.; Chen, A. *J. Magn. Reson. A* **1995**, *115*, 260–264.
(32) (a) Huo, R.; Wehrens, R.; Van Duynhoven, J.; Buydens, L. M. C. *Anal. Chim. Acta* **2003**, *490*, 231–251. (b) Antalek, B.; Hewitt, J. M.; Winding, W.; Yacobucci, P. D.; Mourey, T.; Le, K. *Magn. Reson. Chem.* **2002**, *40*, S60–S71.
(33) Mariette, F.; Guillement, J. P.; Tellier, C.; Marchal, P. In *Signal Treatment and Signal Analysis in NMR*; Rutledge, D. N., Ed.; Elsevier: Amsterdam, The Netherlands, 1996; pp 218−234.
(34) Delsuc, M. A.; Malliavin, T. E. *Anal. Chem.* **1998**, *70*, 2146–2148.
(35) Holz, M.; Mao, X.; Seiferling, D. *J. Chem. Phys.* **1996**, *104*, 669–679.

Table 2. Main Interatomic Distances (Å) for $Sn_{12}O_8(OH)_4(OEt)_{28}(HOEt)_4$[a]

Sn1−O4	1.954(14)	Sn2−O13	1.92(2)	Sn3−O4	1.934(14)	Sn4−O15	1.93(2)
Sn1−O1′	2.036(13)	Sn2−O12	2.050(18)	Sn3−O3	2.063(14)	Sn4−O16	1.970(19)
Sn1−O2	2.090(13)	Sn2−O2	2.058(15)	Sn3−O9	2.068(15)	Sn4−O2	1.987(16)
Sn1−O8	2.104(15)	Sn2−O5	2.079(14)	Sn3−O6	2.071(16)	Sn4−O6	2.092(17)
Sn1−O1	2.109(12)	Sn2−O7′	2.108(14)	Sn3−O10	2.103(15)	Sn4−O14	2.163(16)
Sn1−O7	2.131(13)	Sn2−O1	2.124(13)	Sn3−O5	2.105(13)	Sn4−O8	2.195(15)
Sn5−O18	1.951(17)	Sn5−O3	2.077(15)	Sn6−O21	1.961(19)	Sn6−O11	2.105(17)
Sn5−O17	1.99(2)	Sn5−O10	2.104(16)	Sn6−O20	2.025(16)	Sn6−O9	2.114(15)
Sn5−O11	2.075(19)	Sn5−O19	2.134(16)	Sn6−O3	2.058(15)	Sn6−O22	2.128(17)

[a] Symmetry code: $' = -x, 1 - y, 1 - z$.

Table 3. Complete Assignment of the ^{1}H and ^{13}C NMR Resonances of $Sn_{12}O_8(OH)_4(OEt)_{28}(HOEt)_4$

δ^{13}C (ppm)	δ^1H (ppm)	oxygen	tin[a]
62.70/18.88	4.52 and 4.46/1.56	O7	Sn1 and Sn2′
61.87/18.86	4.69 and 4.52/1.71	O8	Sn1 and Sn4
61.55/18.88	4.46[b]/1.56	O10	Sn3 and Sn5
61.52/19.19	4.58[c] and 4.28[c]/1.59	O9	Sn3 and Sn6
61.46/20.10	4.20 and 4.15/1.35	O21	Sn6
61.43/20.08	4.11/1.37	O18	Sn5
61.38/18.79	4.34 and 4.24/1.51	O11	Sn5 and Sn6
61.00/20.46	4.41/1.47	O15/O16	Sn4
60.60/20.15	4.18[c] and 4.14[c]/1.55	O20	Sn6
60.55/20.18	4.34[b] and 4.25[b]/1.57	O17	Sn5
60.30/19.08	4.36 and 4.21/1.33	O12	Sn2
60.18/20.24	4.42[c]/1.49	O13	Sn2
60.16/20.96	4.51 and 4.44/1.51	O15/O16	Sn4
59.93/17.70	3.95/1.25	O19[d]	Sn5
59.83/17.35	4.20[b] and 4.16[b]/1.42	O14	Sn4
59.70/18.04	3.98/1.20	O22[d]	Sn6
	8.05	O5	Sn2 and Sn3
	7.89	O6	Sn4 and Sn3

[a] δ^{119}Sn (in ppm): −563.5 for Sn1, −625.5 for Sn2, −594.9 for Sn3, −648.7 for Sn4, −607.8 for Sn5, and −609.0 for Sn6. [b] NOE contact with proton Hb at 7.89 ppm. [c] NOE contact with proton Ha at 8.05 ppm. [d] The more shielded methylene moieties, and corresponding methyl groups, have been assigned to O19 and O22, which correspond to an ethoxy/ethanol pair.

3. Results and Discussion

3.1. X-ray Structure of $Sn_{12}O_8(OH)_4(OEt)_{28}(HOEt)_4$. The molecular structure of **1**, as determined from single-crystal X-ray diffraction, is presented in Figure 2. This tin(IV) oxo cluster is centrosymmetric and based on 12 tin atoms, which are all six-coordinate and exhibit distorted octahedral environments. This cluster also contains 44 oxygen atoms, 32 of which correspond to ethoxy moieties, as indicated by the carbon atoms linked to them. Among the ethoxy moieties, which are all located on the surface of the cluster, 22 are terminal and 10 are bridging (μ_2). Among the oxygen atoms that do not correspond to ethoxy moieties, 6 are μ_2 bridges and 6 are μ_3 bridges. The formula derived from the X-ray structure requires eight additional protons to balance its negative charges, but these protons could not be clearly located on the Fourier difference maps. The main interatomic distances are presented in Table 2.

The structure of this elongated dodecameric oxo cluster can be described as being built up from two nonequivalent trimer building blocks (labeled A and B) associated as A−B−B−A. Trimer A, which constitutes each tip of the cluster, is based on Sn3, Sn5, and Sn6 linked together by one μ_3-oxo bridge (O3) and pairwise by three μ_2-ethoxy bridges (O9, O10, and O11). Trimer B is based on Sn1, Sn2, and Sn4 linked together by one μ_3-oxo bridge (O2). In trimer B, Sn1 and Sn2 are also linked by O1 while Sn1 and Sn4 are also linked by O8. The union of trimers B, which forms the central part of the cluster, is achieved through the third bond of two μ_3-oxo bridges (O1 and its symmetric O1′) as well as two μ_2-ethoxy groups (O7 and its symmetric O7′). The connection between trimers A and B is achieved through three μ_2-oxo or hydroxo bridges (O4, O5, and O6 and their symmetric molecules). The main difference between these two trimers is their geometries. Trimer A is based on a trigonal μ_3-oxygen (O3), while trimer B is based on an almost planar μ_3-oxygen (O2), as indicated by the sums of their three Sn−O−Sn angles: 312.2 and 356.8° for O3 and O2, respectively. The 3D packing reveals only van der Waals contacts between the clusters, as expected from the 32 ethoxy moieties that effectively bury the metal−oxo framework below an organic shell.

3.2. Solution-State Study by Multinuclear NMR. Resonance Assignment. In order to locate the eight protons needed to balance the negative charge of the formula derived from the X-ray structure, an extensive multinuclear 1D and 2D NMR investigation was performed at high field. Even at 700 MHz, the ^{1}H NMR spectrum of **1** in C_6D_6 consists of strongly overlapping resonances between 4.7 and 3.9 ppm for the methylene protons and between 1.7 and 1.2 ppm for the methyl protons of the ethoxy groups. The only other contributions in the spectrum are isolated quadruplet and triplet at 3.31 and 0.93 ppm, assigned to ethanol, as well as two singlets at 8.05 and 7.89 ppm, which account each for two protons relative to the 32 ethoxy groups. The broad-band proton-decoupled ^{119}Sn spectrum displays six resonances, showing numerous overlapping ^{119}Sn−$^{119/117}$Sn coupling satellites. In the ^{13}C NMR spectrum, most resonances are resolved but confined into two narrow regions ranging from 63 to 57 ppm and from 23 to 17 ppm.

A ^{1}H−^{13}C HSQC[36] NMR spectrum allows one to distinguish 16 ethoxy methylene carbon atoms and their diastereotopic proton pairs (Figure 3) as well as 16 methyl carbons and their associated protons. Because the cluster has inversion symmetry, these 16 distinct ^{1}H−^{13}C groups of methyl and methylene correlations represent all 32 ethoxy groups of the cluster.

^{1}H−^{119}Sn NMR correlation spectra reported so far in the literature are mostly HMQC-type correlations.[29] Because they are usually recorded without decoupling, they yield $^nJ(^1\text{H}-^{119}\text{Sn})$ couplings that are very informative as to the

(36) (a) Bodenhausen, G.; Ruben, D. J. *Chem. Phys. Lett.* **1980**, *69*, 185–189. (b) Claridge, T. D. W. *High Resolution NMR Techniques in Organic Chemistry*; Elsevier: New York, 2004; pp 229−234.

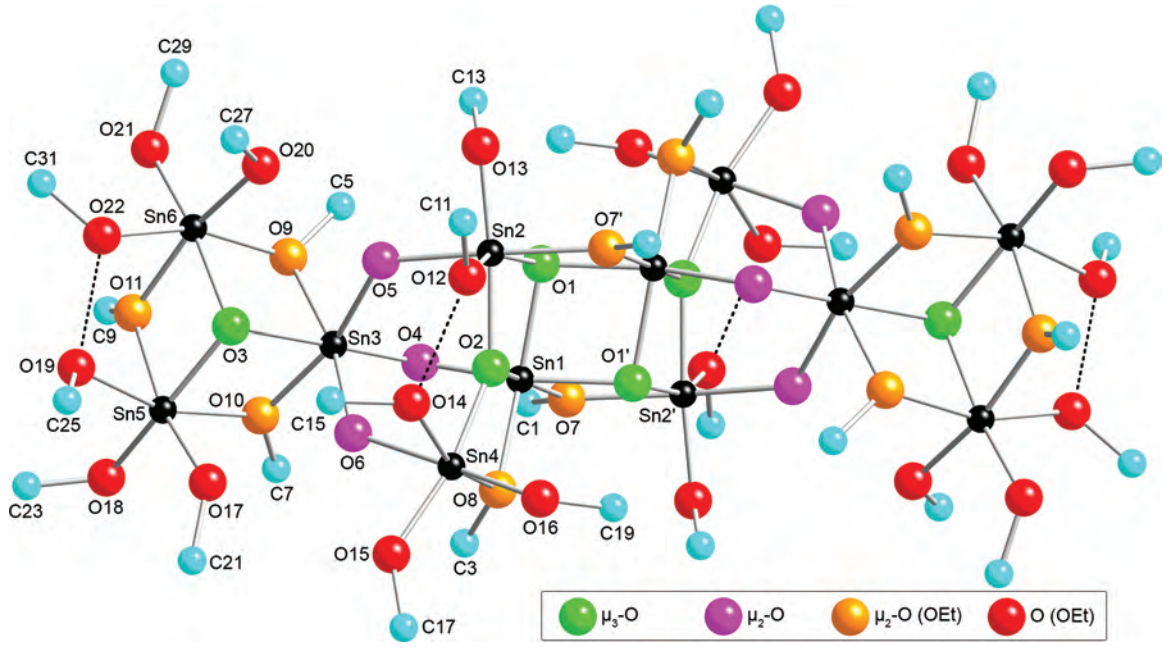

Figure 2. Molecular structure and numbering scheme for $Sn_{12}O_8(OH)_4(OEt)_{28}(HOEt)_4$. For clarity, only the first carbon atom of each ethoxy group is shown.

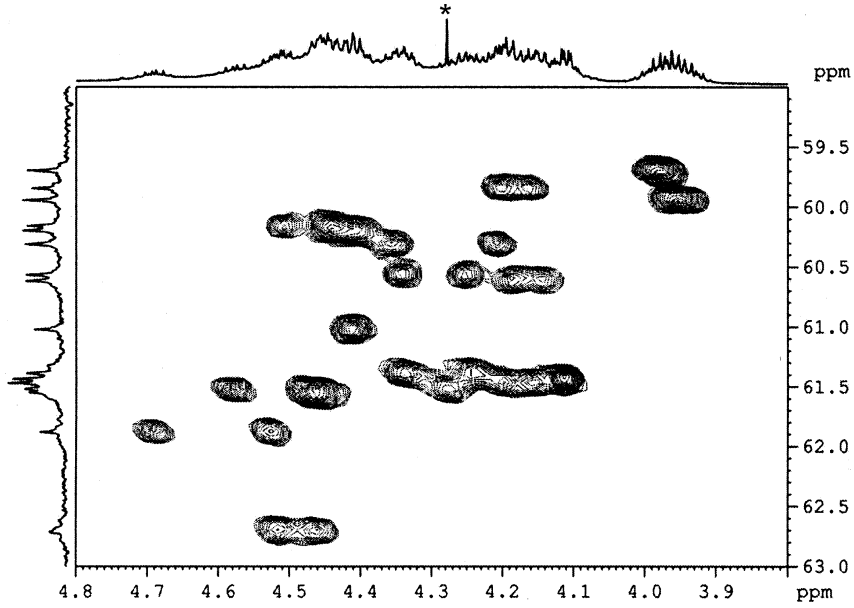

Figure 3. Detail of $^1H-^{13}C$ cross-peaks in the OCH_2 region of the 700 MHz $^1H-^{13}C$ HSQC NMR spectrum of $Sn_{12}O_8(OH)_4(OEt)_{28}(HOEt)_4$ (*: impurity).

structure determination of tin-containing compounds.[37,38] However, the deleterious effects of the phase-twisted line shapes require magnitude-mode processing with strong apodization, thereby reducing the information available in the case of strongly overlapping resonances, as is the case here. A $^1H-^{119}Sn$ HSQC NMR spectrum, which affords phase-sensitive processing, preserves sufficient resolution along the ^1H dimension (see detail in Figure 4) to establish the connectivity pattern associated with the bridging ethoxy groups.

For instance, the ^1H NMR resonance at 4.69 ppm is common to both ^{119}Sn NMR resonances at −563.5 and −648.7 ppm. Because it was established that the ^1H NMR resonance at 4.69 ppm forms a diastereotopic pair with the ^1H NMR resonance at 4.52 ppm (Table 3), which is also common to the latter ^{119}Sn NMR resonances, it can be stated that the two tin atoms associated with these chemical shifts are connected by the bridging ethoxy group bearing the diastereotopic methylene protons at 4.69 and 4.52 ppm. Following this approach, each tin atom, except Sn5 and Sn6, was assigned a chemical shift and each oxygen of the bridging ethoxy groups, except O9 and O10, was associated with the ^1H NMR resonances of its methylene moiety (Figure 5).

(37) Kemmer, M.; Biesemans, M.; Gielen, M.; Tiekink, E. R. T.; Willem, R. *J. Organomet. Chem.* **2001**, *634*, 55–60.
(38) Biesemans, M.; Buytaert, G.; Van Lokeren, L.; Martins, J. C.; Willem, R. *Organometallics* **2003**, *22*, 1888–1893.

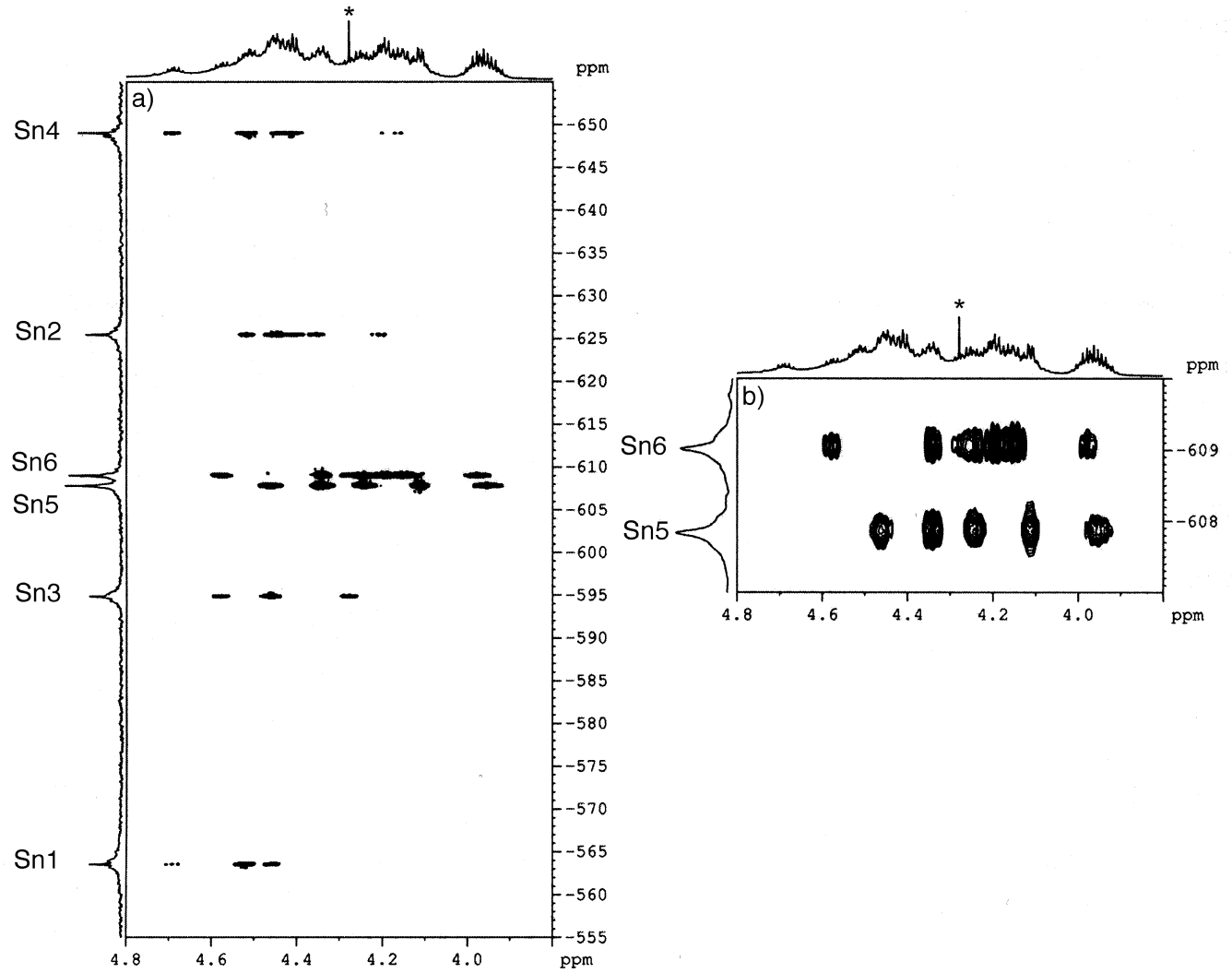

Figure 4. (a) Detail of the ethoxy methylene region of the $^{1}H-^{119}Sn$ HSQC NMR spectrum of $Sn_{12}O_8(OH)_4(OEt)_{28}(HOEt)_4$ (evolution delay of 10 ms). (b) Further expansion of the Sn5−Sn6 region, displaying excellent resolution in the ^{1}H dimension (*: impurity).

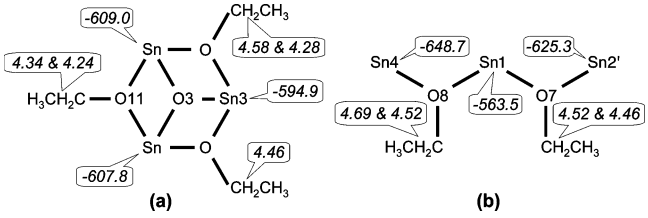

Figure 5. Connectivity pattern as established from $^{1}H-^{119}Sn$ correlations for the bridging ethoxy groups. (^{1}H and ^{119}Sn NMR chemical shifts in ppm.)

In the $^{1}H-^{119}Sn$ HSQC NMR spectrum, the ^{1}H NMR resonance at 8.05 ppm (Ha) shows intense cross-peaks with Sn2 and Sn3 and the ^{1}H NMR resonance at 7.89 ppm (Hb) with Sn3 and Sn4. A nondecoupled $^{1}H-^{119}Sn$ HMQC NMR spectrum (Figure 6) confirms these correlations and establishes that Ha and Hb are both coupled to Sn3 with coupling constants of ca. 17 Hz. According to these observations, Ha was located on O5, between Sn2 and Sn3, and Hb on O6, between Sn3 and Sn4. These protons participate in hydrogen bonding between O5 and O20 (2.73 Å) and O6 and O17 (2.74 Å).

From NOE contacts with Ha or Hb (Table 3), observed in a ROESY NMR spectrum,[39] the assignment of the last two bridging ethoxy groups (O9 and O10) was completed and the tin atoms Sn5 and Sn6 were assigned. With the full assignment of the tin resonances in hand, the terminal ethoxy groups were then assigned from the $^{1}H-^{119}Sn$ HSQC NMR spectrum and NOE contacts with Ha or Hb, assuming that such contacts always involve the closest methylene groups, as estimated from the O5−C or O6−C distances in the solid state.

The pairing of methylene and methyl groups was achieved by a $^{1}H-^{13}C$ HSQC−TOCSY NMR[26] experiment. For the terminal ethoxy groups, this pairing was confirmed by the $^{1}H-^{119}Sn$ HSQC NMR spectrum, in which correlation peaks are observed between the tin atoms and the methyl groups. Such correlations are not observed for bridging ethoxy groups. The complete assignment is summarized in Table 3.

Out of the eight protons required to balance the negative charge of the formula derived from the X-ray structure, four were identified as OH groups by NMR. The four other ones must therefore be localized on some of the ethoxy groups,

(39) Bothner-By, A. A.; Stephens, R. L.; Lee, J.-M.; Warren, C. D.; Jeanloz, R. W. *J. Am. Chem. Soc.* **1984**, *106*, 811–813.

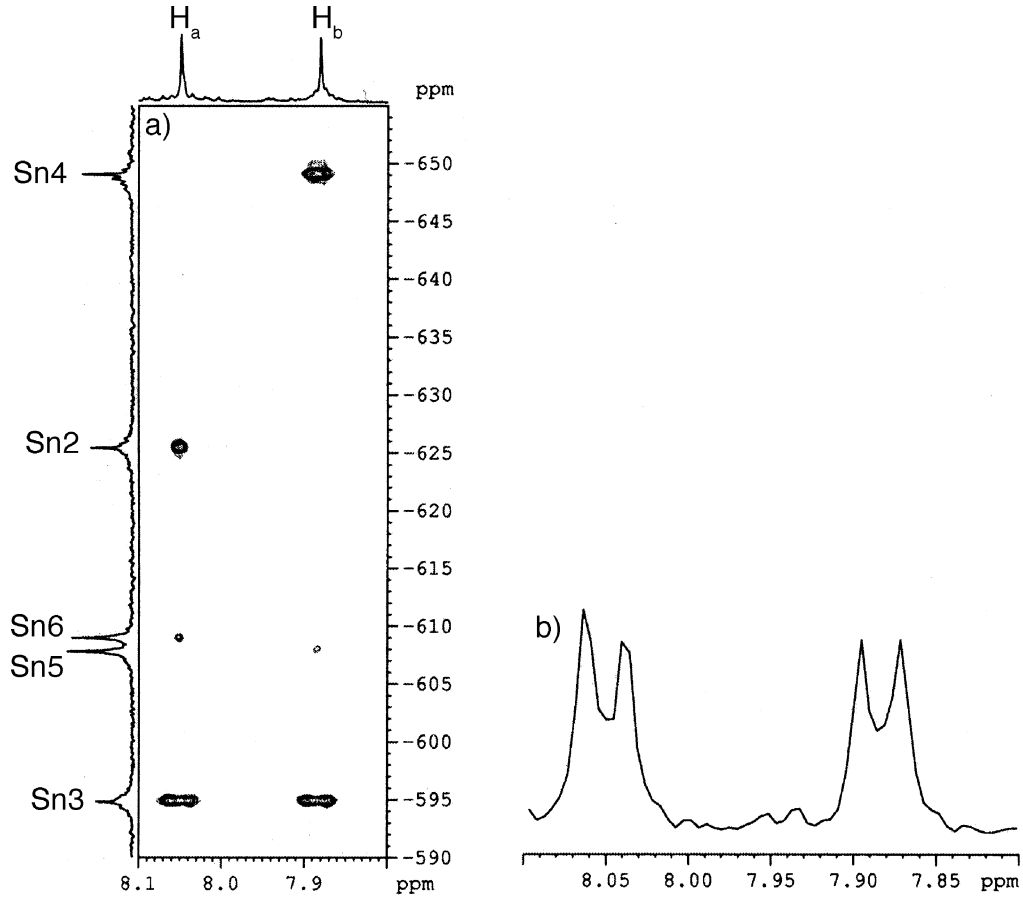

Figure 6. (a) Detail of a nondecoupled $^1H-^{119}Sn$ HMQC NMR spectrum of $Sn_{12}O_8(OH)_4(OEt)_{28}(HOEt)_4$. (b) Cross section through Sn3 allowing one to determine the $^2J(^1H-^{119}Sn)$ coupling constants for both OH protons.

turning them into ethanol ligands bound to tin atoms. Indeed, the formation of a bidentate bridging ligand through the hydrogen bonding of an alkoxy group and an alcohol molecule, located on two neighboring metallic centers, has been observed in several compounds.[40] According to O−O distances, these protons are likely found between O19 and O22 (2.38 Å) and between O12 and O14 (2.45 Å). These O−(H)O contacts are visualized as dotted lines in Figure 2. The long Sn−O distances for O12 (2.05 Å), O14 (2.16 Å), O19 (2.13 Å), and O22 (2.13 Å), compared to the other terminal ethoxy groups on the same tin atoms, as well as the angles O19−Sn5−Sn6 (77.4°) and O22−Sn6−Sn5 (78.5°), smaller than 90°, are additional hints for the presence of these protons.

$^1H-^{13}C$ HMBC NMR spectra,[41] aiming to detect the missing ^2J correlations between these hydroxylic alcohol protons and ethoxy carbon atoms or ^3J correlations between these protons and methyl carbon atoms, were recorded. Using the standard evolution delay of 50 ms for these kinds of experiments, the spectrum is deceptively empty in the ranges 3−5 ppm (^1H)/15−25 ppm (^{13}C) and 3−5 ppm (^1H)/55−65 ppm (^{13}C), lacking in fact any targeted correlation with the methylene carbon atoms. Application of the H2BC pulse sequence, editing specifically heteronuclear $^1H-^{13}C$ two-bond correlations, even for vanishing $^2J(^1H-^{13}C)$ HMQC or HSQC NMR correlations,[42] enabled us indeed to edit all $^2J(^1H-^{13}C)$ correlations between carbon and hydrogen atoms on the neighboring carbon in the ethyl moiety, but no additional correlation involving a hydroxylic hydrogen atom could be detected. Also $^1H-^{119}Sn$ HMQC NMR spectra with longer delays did not reveal the targeted correlations. All of these observations probably find their origin in the exchange equilibrium between free and bound ethanol, as observed in 2D ROESY experiments (vide infra), which constitutes, in fact, an indirect proof of the bound ethanol molecules.

To quantify in a more reliable way the small coupling constants evidenced in the $^1H-^{119}Sn$ HSQC and HMQC NMR spectra, a $^1H-^{119}Sn$ J-HMBC NMR experiment was set up.[43] Using an appropriate set of delays, active couplings in the indirect F1 dimension can be scaled up by a factor κ (23.86 here), while the size of the couplings remains unaffected in F2 (Figure 7). This upscaling has two advan-

(40) (a) Tolédano, P.; Ribot, F.; Sanchez, C. *Acta Crystallogr., Sect. C* **1990**, *46*, 1419–1422. (b) Vaartstra, B.; Daran, J.-C.; Gradeff, P. S.; Hubert-Pfalzgraf, L. G.; Huffman, J. C.; Parraud, S.; Yunlu, K.; Caulton, K. G. *Inorg. Chem.* **1990**, *29*, 3126–3131. (c) Hampden-Smith, M. J.; Wark, T. A.; Rheingold, A.; Huffman, J. C. *Can. J. Chem.* **1991**, *69*, 121–129. (d) Fric, H.; Schubert, U. *New J. Chem.* **2005**, *29*, 232–236.

(41) (a) Bax, A.; Summers, M. F. *J. Am. Chem. Soc.* **1986**, *108*, 2093–2094. (b) Summers, M. F.; Marzilli, L. G.; Bax, A. *J. Am. Chem. Soc.* **1986**, *108*, 4285–4294.

(42) (a) Nyberg, N. T.; Duus, J. Œ.; Sœrensen, O. W. *J. Am. Chem. Soc.* **2005**, *127*, 6154–6155. (b) Nyberg, N. T.; Duus, J. Œ.; Sœrensen, O. W. *Magn. Reson. Chem.* **2005**, *43*, 971–974.

(43) Meissner, A.; Sœrensen, O. W. *Magn. Reson. Chem.* **2001**, *39*, 49–52.

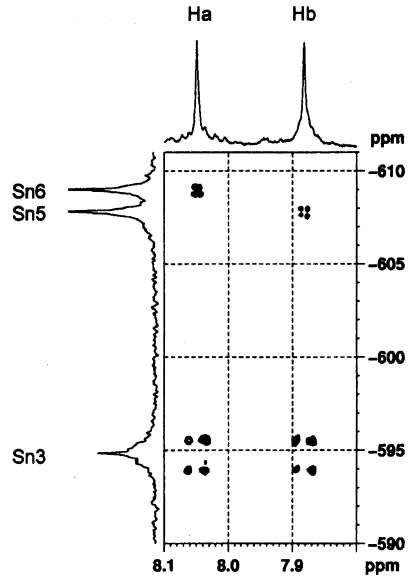

Figure 7. Detail of a $^{1}H-^{119}Sn$ J-HMBC NMR spectrum of $Sn_{12}O_8(OH)_4(OEt)_{28}(HOEt)_4$ illustrating scaled $^{n}J(^{1}H-^{119}Sn)$ coupling constants in the F1 dimension (scaling factor = 23.86).

tages. First, the absolute error on the measured coupling constant is reduced as larger scaling factors are used. Second, because the splitting of the antiphase doublets in F1 greatly exceeds the peak line width, an accurate measurement of the coupling can be performed because no error due to peak cancelation is expected. The results of this experiment are summarized in Table 4. Thus, for all of the terminal ethoxy groups, except O14, the $^{4}J(^{1}H-^{119}Sn)$ couplings between the respective tin nuclei and the methyl protons, as well as the $^{2}J(^{1}H-^{119}Sn)$ and $^{4}J(^{1}H-^{119}Sn)$ couplings of the OH protons, are quantified. Actually, these last $^{4}J(^{1}H-^{119}Sn)$ couplings are combined with $^{2}J(^{1}H-^{119}Sn)$ through O5(H)−O20 and O6(H)−O17 hydrogen bonding. This feature explains why no $^{4}J(^{1}H-^{119}Sn)$ is detected between Ha and Sn5 and between Hb and Sn6. Even some of the $^{3}J(^{1}H-^{119}Sn)$ correlations between tin and the methylene protons were obtained, although the experiment was optimized in order to edit preferentially small couplings.

Once all of the ^{1}H and ^{13}C NMR resonances have been assigned, some comments can be made in relation with the molecular structure. As was already observed for $Ti_{16}O_{16}(OEt)_{32}$ and $Zr_4(O^nPR)_{16}$,[15,44] bridging and terminal alkoxy groups cannot be distinguished on the basis of their ^{1}H or ^{13}C NMR chemical shifts. Indeed, the ^{13}C or ^{1}H NMR chemical shift ranges associated with terminal and bridging alkoxy groups overlap (Table 3). This overlap is minor for the ^{13}C NMR resonances associated with the α-CH_2 of the ethoxy groups, yet it rules out any possible assignment purely based on the nature (bridging vs terminal) of the alkoxy groups. There is also no apparent correlation between the Sn−O distances and the ^{13}C or ^{1}H NMR chemical shifts of the α-CH_2 of the ethoxy groups.

Concerning $^{3}J(^{1}H-^{119}Sn)$ (Table 4), the ranges observed for bridging (31.1−48.0 Hz) and terminal (29.7−51.0 Hz) ethoxy groups are superimposed and the observation made in a series of carboxylate-modified tin(IV) isopropoxides, $[Sn(O^iPr)_2(O_2CR)_2]_2$ [R = $(CH_3)CCH_2$, C_6H_5, CH_3],[45] for which the coupling constants associated with terminal alkoxy groups are larger than the ones associated with bridging alkoxy groups, is not verified for $Sn_{12}O_8(OH)_4(OEt)_{28}$-$(HOEt)_4$. Interestingly, the $^{4}J(^{1}H-^{119}Sn)$ scalar couplings, which involve the protonated ethoxy groups, are among the smallest observed in **1**.

ROESY Exchange Peak Analysis. Interestingly, the ROESY NMR spectrum also displays exchange cross-peaks, having opposite sign with respect to the NOE peaks,[46] which reveal the presence of cluster ligand-exchange phenomena. Because of the high degree of overlap and interference from cross-relaxation ROESY peaks, any quantitative exchange cross-peak volume determination is unrealistic and was not attempted. Some cross-peak assignments are even ambiguous. Nevertheless, a number of trends as to which cluster ligands undergo preferential exchange phenomena, as well as on the nature of the latter, can be observed.

For short mixing times (25, 50, and 100 ms), strong exchange cross-peaks that involve the diastereotopic proton pair within each individual methylene group are observed. This feature is especially evident for the pairs with the larger chemical shift differences (i.e., 4.69 and 4.52 ppm on O8, 4.58 and 4.28 ppm on O9, 4.34 and 4.24 ppm on O11, and 4.36 and 4.21 ppm on O12). Significantly weaker cross-peaks are also observed between the free ethanol and several ethoxy groups. A detailed assignment of the latter is impossible, but the bridging ethoxy groups related to O8 and O9 are clearly not involved because the cross-peaks with free ethanol are all below 4.5 ppm. These unexpected results can only be interpreted by a dissociation−reassociation mechanism of the ethoxy groups, causing the diastereotopic protons of the prochiral methylene carbon to become equivalent, within each of these ligands, on the 2D exchange time scale. This mechanism does not need to involve free ethanol, as is clearly observed for the bridging ethoxy groups related to O8 and O9.

Remarkably, at these mixing times (25, 50, and 100 ms), no cross-peaks directly correlating resonances from different ligands, either bridging or terminal, whether hydroxylated or not, are observed, clearly indicating that at short mixing times only dissociation−reassociation and intermolecular exchange with free ethanol are significantly operational, with the former being slightly faster than the latter. These general trends are confirmed in a ROESY NMR experiment with a mixing time of 225 ms, where only scarce cross-peaks correlate directly different ligands, while nearly all cluster ligands display exchange cross-peaks with free ethanol.

The general conclusion from these EXSY data of the 2D ROESY NMR spectra is that whenever the mixing time is taken as long enough, exchange of essentially all ligands with free ethanol becomes observable and that mutual cluster

(44) Day, V. W.; Klemperer, W. G.; Pafford, M. M. *Inorg. Chem.* **2001**, *40*, 5738–5746.
(45) Martinez-Ferrero, E.; Boubekeur, K.; Ribot, F. *Eur. J. Inorg. Chem.* **2006**, 802–807.
(46) Olejniczak, E. T.; Hoch, J. C.; Dobson, C. M.; Poulsen, F. M. *J. Magn. Reson.* **1985**, *64*, 199–206.

Table 4. $^nJ(^1H-^{119}Sn)$, As Determined from the J-HMBC Experiment for $Sn_{12}O_8(OH)_4(OEt)_{28}(HOEt)_4$

oxygen	type	δ^1H (OH or OCH_2) [$^nJ(^1H-^{119}Sn)$][a]	δ^1H (CH_3) [$^4J(^1H-^{119}Sn)$][a]
O5	μ-OH	8.05 [3.9 with Sn2, 17.3 with Sn3, 4.0 with Sn6]	
O6	μ-OH	7.89 [16.6 with Sn3, 11.0 with Sn4, 3.8 with Sn5]	
O7	μ-OEt	4.52 [33.2 with Sn2′] and 4.46 [35.6 with Sn2′]	1.56
O8	μ-OEt	4.69 and 4.52	1.71
O9	μ-OEt	4.58 [44.6 with Sn6] and 4.28 [48.0 with Sn6]	1.59
O10	μ-OEt	4.46 [34.8 with Sn5]	1.56
O11	μ-OEt	4.34 and 4.24	1.51
O12	(H)OEt	4.36 [41.9 with Sn2] and 4.21 [31.1 with Sn2]	1.33 [4.7 with Sn2]
O13	OEt	4.42 [29.7 with Sn2]	1.49 [11.6 with Sn2]
O14	(H)OEt	4.20 and 4.16	1.42
O15/O16	OEt	4.41	1.47 [7.7 with Sn4]
O15/O16	OEt	4.51 and 4.44	1.51 [8.2 with Sn4]
O17	OEt	4.34 and 4.25	1.57 [5.0 with Sn5]
O18	OEt	4.11	1.37 [9.9 with Sn5]
O19	(H)OEt	3.95	1.25 [3.3 with Sn5]
O20	OEt	4.18 and 4.14	1.55 [4.2 with Sn6]
O21	OEt	4.20 [35.4 with Sn6] and 4.15 [51.0 with Sn6]	1.35 [9.9 with Sn6]
O22	(H)OEt	3.98	1.20 [3.8 with Sn6]

[a] δ in ppm and ^nJ in Hz.

ligand exchange must essentially be mediated by free ethanol. However, even at only 225 ms, the overlap with nearby intense ROESY cross-peaks becomes too important. As a result, any ROESY NMR spectrum recorded with longer mixing time fails to document whether all cluster ligands can undergo direct or only relayed exchange with free ethanol.

DOSY Analysis. DOSY NMR,[47] which gives access to translational diffusion coefficients, is a valuable tool in organometallic and inorganic chemistry.[48] According to its solid-state structure, the shape of the cluster is reasonably well approximated by a prolate ellipsoid with minor and major semiaxes of 7.00 and 11.75 Å, respectively. From this, its diffusion coefficient can be estimated at 4.7×10^{-10} m^2/s, using the Stokes−Einstein equation corrected by a shape factor for prolate ellipsoids (eq 1), where k_B is Boltzmann's constant, T is the absolute temperature, η is the viscosity of the medium, a and b are the major and minor semiaxes, respectively, and ρ is the axial ratio (a/b).[49]

$$D = \frac{k_B T}{6\pi\eta b} \frac{\ln(\rho + \sqrt{\rho^2 - 1})}{\sqrt{\rho^2 - 1}} \quad (1)$$

Figure 8 displays the diffusion coefficient measured for the cluster and for the "free" ethanol as a function of the diffusion delay ranging from 25 to 400 ms in the BPP-LED pulse sequence. The diffusion coefficient of the "free" ethanol decreases with increasing diffusion delay, confirming the exchange phenomenon with the cluster, as was already revealed above by the 2D ROESY data.

On the other hand, the diffusion coefficients measured for the ethoxy resonances increase with increasing diffusion delay. Moreover, for a given value of the diffusion delay, they are identical, within experimental uncertainty, for the

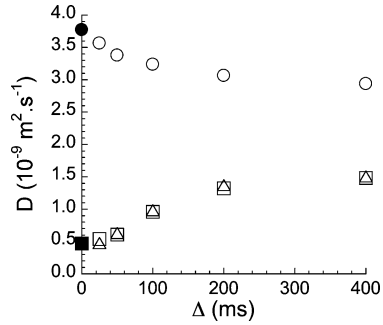

Figure 8. Dependence of the diffusion coefficient on the diffusion delay (Δ) used in the BPP-LED pulse sequence: "free" ethanol (open circles); OCH_2CH_3 (open squares); OCH_2CH_3 (open triangles). The solid circle corresponds to the diffusion coefficient (3.77×10^{-9} m^2/s) measured for a blank solution of diluted ethanol in benzene-d_6. The solid square corresponds to the estimation of the diffusion coefficient of the cluster from eq 1.

CH_2 and CH_3 resonances and for all of the ligands of the cluster. Stated in other terms, no particular cross-peak associated with cluster ethoxy or ethanol ligands exhibits any stronger or weaker increase in the diffusion coefficient value than any other one. The 2D DOSY cross-peaks of "free" ethanol as well as of the cluster do not evolve toward mutual coalescence along the diffusion time scale upon increasing diffusion delay but rather each tends to an asymptotic constant value at the highest measured diffusion delay (400 ms). These observations indicate that, as for the 2D ROESY spectra where the exchange between "free" ethanol and cluster ligands is moderately slow (i.e., in precoalescence, on the chemical shift time scale), the exchange is also moderately slow on the diffusion time scale. This can be expected because the time scales are of the same order of magnitude, with the ROESY mixing time range being 25−225 ms, while in the DOSY spectra, the diffusion delay range covered is 25−400 ms.[50] Because of the multisite character of the exchange and the fact that the measured diffusion coefficients are therefore apparent and heavily affected by exchange in the moderately slow exchange

(47) Johnson, C. S., Jr. *Prog. Nucl. Magn. Reson. Spectrosc.* **1999**, *34*, 203–256.
(48) Pregosin, P. S. *Prog. Nucl. Magn. Reson. Spectrosc.* **2006**, *49*, 261–288.
(49) (a) Hiemenz, P. C. *Principles of Colloid and Surface Chemistry*, 2nd ed.; Marcel Dekker Inc.: New York, 1986. (b) Balinov, B.; Ollson, U.; Söderman, O. *J. Phys. Chem.* **1991**, *95*, 5931–5936.
(50) (a) Johnson, C. S., Jr. *J. Magn. Reson., Ser. A* **1993**, *102*, 214–218. (b) Cabrita, E. J.; Berger, S.; Bräuer, P.; Kärger, J. *J. Magn. Reson.* **2002**, *157*, 124–131.

regime where their mathematical dependence on rate exchange parameters is complex,[50] no attempt was made to process these apparent diffusion coefficients quantitatively in order to deduce rate constants.

However, the qualitative exchange information deduced from ROESY and DOSY experiments appears to be complementary. The 2D ROESY EXSY NMR peaks provide information as to exactly which kind of exchange occurs, indicating also clearly, even though only qualitatively, differences in rate constant ranges, information that the 2D DOSY NMR peaks fail to provide. Thus, the 2D DOSY peaks only provide more global information, revealing that, at sufficiently long exchange delays, all cluster ligands finally get exchanged, either directly or relayed, with free ethanol, because all cluster resonances globally show the same apparent diffusion coefficient at a given diffusion delay value. The latter qualitative exchange information is, in principle, accessible in 2D ROESY NMR spectra at long mixing times but could not be obtained unambiguously for the cluster, as a consequence of the increasing overlapping and complexity degree upon increasing mixing time.

4. Conclusion

The tin(IV) oxoethoxo cluster, $Sn_{12}O_8(OH)_4(OEt)_{28}(HOEt)_4$, has been obtained by substoichiometric hydrolysis of $[Sn(O^iPr)_4 \cdot HO^iPr]_2$ in ethanol ($H_2O/Sn = 0.5$). This new member in the family of dodecameric oxo clusters has been characterized by X-ray diffraction. Its structure, which includes only six-coordinate metallic centers, is formed from two different types of trimeric subunits. The resulting metal−oxo framework is elongated and exhibits ethoxy groups on its surface.

In spite of the extreme degree of overlap and resonance pattern complexity in the ^1H NMR spectrum, even at 700 MHz, all ^{119}Sn, ^1H, and ^{13}C NMR resonances in solution could be assigned, using various complementary homo- and heteronuclear correlation techniques. Moreover, NMR spectroscopy, and more particularly $^1H-^{119}Sn$ HSQC NMR, used for the first time to the best of our knowledge, has allowed us to locate hydrogen atoms, not seen by X-ray diffraction, on the metal−oxo framework. All of these NMR results show that the structure observed in the solid state is fully preserved in solution. Yet, complementary 2D exchange data and 2D diffusion data revealed dissociation−reassociation phenomena as well as moderately slow exchange with free ethanol present in the sample.

Acknowledgment. E.M.-F. thanks the European Community for a postdoctoral contract under the Human Potential Program (HPRNT-CT-2002-00306, NBB-Hybrids). M.B., R.W., and J.C.M. are indebted to the Fund for Scientific Research-Flanders (Belgium) for financial support in several grants (Grants G.0016.02, G.0469.06, and G.0064.07). The FWO Scientific Research Network on Magnetic Resonance is gratefully acknowledged for financially facilitating exchange of researchers between the different laboratories involved in this work (Grant WO.01407). R.W. is indebted to the Research Council (Onderzoeksraad) of the Vrije Universiteit Brussel for financial support (Concerted Research Action, Grant GOA31 and other grants). The IWT Flanders is thanked for a SBO-Ph.D. grant to P.M.S.H. The 700 MHz equipment of the Interuniversitary NMR Facility was financed from the "Zware Apparatuur FFEU" incentive of the Flemish Government, by Universiteit Gent, Vrije Universiteit Brussel, and Universiteit Antwerpen. E.M.-F. and F.R. thank Dr. L. Rozes for fruitful discussions on the naming of oxo clusters.

Supporting Information Available: Crystallographic data of $Sn_{12}O_8(OH)_4(OEt)_{28}(HOEt)_4$ (CIF and drawing with thermal ellipsoids). This material is available free of charge via the Internet at http://pubs.acs.org.

IC800123Z